Magnetic Resonance Imaging 58 (2019) 56–66

Contents lists available at ScienceDirect

Magnetic Resonance Imaging

journal homepage: www.elsevier.com/locate/mri

Original contribution

Sliding motion compensated low-rank plus sparse (SMC-LS) reconstruction for high spatiotemporal free-breathing liver 4D DCE-MRI

Wenyuan Qiu[a], Dongxiao Li[a,*], Xinyu Jin[a], Fan Liu[a], Thanh D. Nguyen[b], Martin R. Prince[b], Yi Wang[b,c], Pascal Spincemaille[b]

[a] College of Information Science and Electronic Engineering, Zhejiang University, Hangzhou, China
[b] Department of Radiology, Weill Cornell Medical College, New York, NY, United States
[c] Department of Biomedical Engineering, Cornell University, Ithaca, NY, United States

ARTICLE INFO

Keywords:
Liver
DCE-MRI
Free breathing
Sliding motion
Low-rank plus sparse

ABSTRACT

Liver dynamic contrast-enhanced MRI (DCE-MRI) requires high spatiotemporal resolution and large field of view to clearly visualize all relevant enhancement phases and detect early-stage liver lesions. The low-rank plus sparse (L + S) reconstruction outperforms standard sparsity-only-based reconstruction through separation of low-rank background component (L) and sparse dynamic components (S). However, the L + S decomposition is sensitive to respiratory motion so that image quality is compromised when breathing occurs during long time data acquisition. To enable high quality reconstruction for free-breathing liver 4D DCE-MRI, this paper presents a novel method called SMC-LS, which incorporates Sliding Motion Compensation into the standard L + S reconstruction. The global superior-inferior displacement of the internal abdominal organs is inferred directly from the undersampled raw data and then used to correct the breathing induced sliding motion which is the dominant component of respiratory motion. With sliding motion compensation, the reconstructed temporal frames are roughly registered before applying the standard L + S decomposition. The proposed method has been validated using free-breathing liver 4D MRI phantom data, free-breathing liver 4D DCE-MRI phantom data, and in vivo free breathing liver 4D MRI dataset. Results demonstrated that SMC-LS reconstruction can effectively reduce motion blurring artefacts and preserve both spatial structures and temporal variations at a sub-second temporal frame rate for free-breathing whole-liver 4D DCE-MRI.

1. Introduction

Liver dynamic contrast-enhanced MRI (DCE-MRI) can not only provide morphological information of liver lesions, but also visualize micro-circulation changes in blood supply, both of which are crucial to the accurate diagnosis of liver diseases in early stage. For successful application of liver DCE-MRI in clinical diagnosis, high spatial resolution with large coverage is required to detect small lesions inside the whole liver, and high temporal resolution with long scan time is also required to accurately track contrast enhancement patterns [1].

High spatiotemporal whole-liver 4D DCE-MRI remains an open problem, of which the major technical difficulty is fast imaging. A lot of research on fast MRI has been reported in the literature. Parallel imaging techniques using arrays of receiver coils with spatially varying sensitivities were firstly proposed for fast imaging, e.g. SMASH [2], SENSE [3], and GRAPPA [4]. Spatiotemporal correlations were exploited in addition to speed up imaging, e.g. k-t BLAST [5], k-t SENSE [6], and k-t GRAPPA [7]. Efficient acquisition schemes, such as radial sampling [8] and spiral sampling [9], have been introduced to further accelerate parallel imaging.

Compressed sensing theory-based image reconstruction has been the main driving force for dynamic MRI in the last decade. Various techniques have been explored for high quality image reconstruction using vastly undersampled raw data by exploiting the sparsity of MR signal in image domain or in some transform domains [10–16]. Recently, in addition to sparsity, low rank features have been exploited to improve dynamic MRI reconstruction [17–20]. Among them, the low-rank plus sparse (L + S) matrix decomposition [19] model was introduced to reconstruct undersampled dynamic MRI as a superposition of low-rank background component and sparse dynamic component. Compared to standard sparsity-only-based reconstruction methods, the L + S decomposition model increased the compressibility of dynamic MRI data and thus enabled high spatiotemporal reconstruction with high acceleration factors [19]. Recently, Ravishankar et al. proposed a

* Corresponding author at: College of Information Science and Electronic Engineering, Zhejiang University, 38 Zheda Road, Hangzhou 310027, China.
E-mail address: lidx@zju.edu.cn (D. Li).

https://doi.org/10.1016/j.mri.2019.01.012
Received 6 September 2018; Received in revised form 6 December 2018; Accepted 12 January 2019

low-rank and adaptive sparse signal model (LASSI) [20] for highly accelerated dynamic imaging where the sparse component is divided into overlapping spatiotemporal 3D patches, which are sparsely encoded with adaptively learned dictionary. Numerical experiments demonstrated the promising performance of LASSI in dynamic MRI reconstruction compared to the conventional dictionary-blind compressed sensing and L + S reconstruction methods.

However, all the reconstruction methods mentioned above, including the standard L + S reconstruction [19] and LASSI reconstruction [20], are sensitive to respiratory motion, which causes spatial misalignment among temporal frames and consequently breaks down spatiotemporal correlations. Image reconstruction quality is compromised by ghosting artefacts when breathing occurs during long time data acquisition [21,22]. Multiple breath-holds protocol [23,24] has been widely used for the reduction of respiratory motion artefacts. Nevertheless, breath-holding capability is generally compromised for patients, elderly people, and young children. Moreover, breath-holding position often drifts between successive breath-holds. Therefore, image reconstruction has to be carried out for each breath-hold period separately which lowers the utilization of temporal correlation.

In contrast to multiple breath-holds, free breathing [25] is an ideal, easy to follow protocol which allows the subject to breathe quietly and uninterruptedly in a natural way. Various approaches have been investigated for free breathing 4D MRI reconstruction, but most of them are on cardiac imaging [26–31]. However, we found in practice that those reconstruction methods developed for free-breathing cardiac 4D MRI did not work well for free-breathing liver 4D MRI. The main cause is probably that the systolic and diastolic cardiac motion is small and rhythmic, and the maximal displacement of the heart due to breathing is about 8 mm [32], whereas the maximal range of respiratory sliding motion of the liver in extreme cases could reach 80 mm [33].

Fortunately, the standard L + S decomposition model is still capable to achieve high spatiotemporal 4D MRI reconstruction with acceptable quality when the motion magnitude is small, typically in cardiac imaging [19]. To cope with respiratory motion in free-breathing abdominal imaging, Otazo et al. attempted to incorporate an optical flow-based deformable model into the L + S formulation to align all the temporal frames iteratively during image reconstruction [34]. At each iteration, low rank and sparsity are enforced on the registered version of L and S components, data consistency is enforced on the unregistered image reconstructions, and motion vectors are updated along with image updates. However, the convergence of iterative alternating optimization of image reconstruction and motion field estimation is not guaranteed.

Recently, Zhang et al. [35] proposed a soft-gating approach to reduce respiratory motion blurring artefacts by incorporating a motion-weighting function obtained from acquired raw data into the data consistency term to enforce a weighted data consistency. Those data points with more motion are assigned with smaller data consistency weighting. Feng et al. [36] proposed a novel framework for free-breathing 4D MRI called XD-GRASP, which sorts the raw data into extra respiratory motion state dimensions using the self-navigation properties of radial sampling, and then reconstructs a composite image for each motion state separately using compressed sensing. Ghosting artefacts could be effectively reduced in each composite image but at the expense of reduced temporal resolution to ~13 s [36].

To enable free-breathing whole-liver 4D DCE-MRI reconstruction with high spatiotemporal resolution and high quality, this paper presents a novel method called SMC-LS, which incorporates respiratory Sliding Motion Compensation into the standard L + S reconstruction. In abdominal imaging, respiration results in a dominant superior-inferior sliding motion of the internal organs – such as the liver – against the inward-outward moving abdominal wall and the stationary spine [33]. In contrast to using a complicated non-rigid motion model [34], we only correct the respiratory motion of the internal abdominal organs with a global superior-inferior displacement, which is inferred directly from the acquired k-space data. The rationale of SMC-LS is based on the assumption that after compensation of the dominant sliding motion, the reconstructed temporal frames can be roughly registered, and therefore the spatiotemporal correlations can be well recovered for successful application of the standard L + S decomposition. The validation of the proposed method is demonstrated using free breathing liver 4D MRI phantom data and in vivo data with comparisons to the standard L + S reconstruction and XD-GRASP.

2. Theory

2.1. Standard L + S reconstruction model

The L + S approach aims to decompose a matrix $\mathbf{M}$ to a low-rank component $\mathbf{L}$ and a sparse component $\mathbf{S}$ by solving the following convex optimization problem [37]:

$$\min_{\mathbf{L},\mathbf{S}} \|\mathbf{L}\|_* + \lambda \|\mathbf{S}\|_1 \quad \text{s. t.} \quad \mathbf{M} = \mathbf{L} + \mathbf{S} \tag{1}$$

where $\|\mathbf{L}\|_*$ is the nuclear norm of matrix $\mathbf{L}$, $\|\mathbf{S}\|_1$ is the l_1 norm of matrix $\mathbf{S}$, and λ is a tuning parameter used to balance the contribution between $\mathbf{L}$ and $\mathbf{S}$. Otazo et al. firstly introduced the L + S decomposition model into DCE-MRI reconstruction by formulating the reconstruction as the following optimizing problem [19]:

$$\min_{\mathbf{L},\mathbf{S}} \frac{1}{2} \|\mathbf{E}(\mathbf{L} + \mathbf{S}) - \mathbf{d}\|_2^2 + \lambda_L \|\mathbf{L}\|_* + \lambda_S \|\mathbf{TS}\|_1 \tag{2}$$

where $\boldsymbol{L} + \boldsymbol{S}$ is a spatiotemporal matrix in which each column vector corresponds to a temporal image frame reconstruction, $\boldsymbol{T}$ is a sparsifying transform (e.g. Fourier transform (FT), total variation, etc.), $\boldsymbol{d}$ is the acquired raw data defined as a stretched-out single column vector, and $\boldsymbol{E}$ is given by the frame-by-frame multi-coil encoding operator, which performs a multiplication by coil sensitivities followed by an undersampled FT for data acquisition with multiple receiver coils, and λ_L, λ_S are corresponding regularization parameters. Hence the reconstructed images are represented as a superposition of low-rank background ($\boldsymbol{L}$) and dynamic components ($\boldsymbol{S}$).

2.2. Respiratory sliding motion estimation

In natural free breathing, the internal abdominal organs undergo a superior-inferior sliding motion plus free form deformation, while the abdominal wall moves a little bit in-wards and out-wards, and the back bone remains stationary. The respiratory motion filed in abdominal imaging is very complicated, but fortunately in natural free breathing the one dimensional superior-inferior sliding motion constitutes the dominant component, whereas the magnitude of the residue motion is small. Therefore, in this work we propose to use a simplified respiratory motion model, which only estimates a scalar value – the global displacement of superior-inferior sliding motion – from the acquired raw data.

According to the definition of 2D DFT, the k-space origin data of an axial slice, which represents the zero frequency or direct current (DC) component, is proportional to the mean intensity of the slice. The k-space origin data of all axial slices of one temporal frame form a projection of the volume onto the z (superior-inferior) axis. The global displacement of these axial slices can be derived as the center of mass of this z-intensity projection profile [25].

However, only the internal organs are sliding. To exclude the external regions from sliding motion, we extract a motion mask by manually segment the sliding interface in a composite image using ITK-SNAP [38]. The composite image is a sliding window reconstruction using all the acquired k-space data. This over-sampled composite image is blurry in the internal regions due to large motion but is sharp in the external motionless regions, which is sufficient for manual segmentation of the sliding motion mask.

We assume that the external part outside of the sliding interface keeps nearly static during free-breathing liver DCE-MRI acquisition and the corresponding area in the composite image is a good estimate for this part. The k-space origin data of the internal part of each axial slice is calculated by subtracting the zero frequency of the external part of the composite image from the acquired k-space origin data of that slice. The result k-space origin data of all axial slices of the same temporal frame form a z-intensity projection profile (ZIP) of the internal sliding part. The global displacement of sliding motion is estimated by applying a group-wise rigid registration to the ZIP sequence using Demons [39]. The ZIP of the first frame is set as the reference in group registration, and only one motion parameter – the global superior-inferior displacement – is estimated.

For parallel imaging using multiple coils, the global displacement of respiratory sliding motion is estimated separately for each coil using the above method. Then the results are combined using the coil clustering method proposed in [40] to determine the dominant motion. In DCE-MRI, the temporal variation of the ZIP sequence results from not only the sliding motion but also the contrast enhancement. In this work, the contrast enhancement is separated from the respiratory sliding motion by subtracting its envelope, which is estimated using a spline data fitting procedure [36].

2.3. SMC-LS reconstruction

In SMC-LS, free-breathing liver 4D DCE-MRI reconstruction is formulated as the following optimization problem:

$$\min_{\{\mathbf{L}_i,\mathbf{S}_i\}_{i=1}^n} \sum_{i=1}^{n} \left(\lambda_{\mathrm{L}} \|\mathbf{L}_i\|_* + \lambda_{\mathrm{S}} \|\mathbf{T}\mathbf{S}_i\|_1\right) + \frac{1}{2} \left\| \mathbf{E}\left(\tau \sum_{i=1}^{n} \mathbf{R}_i(\mathbf{L}_i + \mathbf{S}_i)\right) - \mathbf{D} \right\|_2^2 \tag{3}$$

where the first part exploits low rank and sparsity of the reconstructed volumetric images, and the second part enforces data consistency. n is the number of axial slices, $\mathbf{L}_i$ is the low-rank component and $\mathbf{S}_i$ is the sparse component of the spatiotemporal matrix of axial slice i in the reconstructed 4D image after inter-frame sliding motion compensation, $\mathbf{T}$ is the total variation operator which enforces sparsity, $\lambda_{\mathbf{L}}$ and $\lambda_{\mathbf{S}}$ are regularization parameters. $\mathbf{E}$ denotes the k-space data acquisition operator, which performs a multiplication by multi-channel coil sensitivities followed by an undersampled Fourier transform, and $\mathbf{D}$ denotes the acquired multi-coil raw data. $\mathbf{R}_i$ is an operator that assembles the superposition of $\mathbf{L}_i$ and $\mathbf{S}_i$ back into the registered 4D image. τ is an image transformation operator that models respiratory sliding motion, which globally shifts the internal abdominal organs in superior-inferior direction frame by frame using the estimated displacement signal, while the external region outside of the sliding interface keeps static. The same sliding motion mask, which was manually annotated in sliding motion estimation, is reused in motion transformation τ for all the temporal frames. By introducing sliding motion compensation into the standard L + S model, the low-rank and sparsity constraints in SMC-LS are enforced on a roughly registered version of the reconstructed 4D image with recovered spatiotemporal correlations.

To solve Eq. (3), consider the following optimization problem:

$$\min_{x} \; g(x) + h(x) \tag{4}$$

where $g(x)$ is convex and smooth, and $h(x)$ is convex but not necessarily smooth. The proximal gradient method takes the form:

$$x_k = prox_h(x_{k-1} - t_k \nabla g(x_{k-1})) \tag{5}$$

where t_k is a sequence of step sizes and $prox_h$ is the proximity function for $h(x)$. The proximity function is soft thresholding of the singular values when $h(x)$ is the nuclear norm or is given by soft thresholding of coefficients when $h(x)$ is l_1 norm.

In our work, $\mathbf{L}_i$ and $\mathbf{S}_i$ in Eq. (3) are optimized iteratively as follows:

$$\begin{aligned}
\mathbf{L}_i^k &= \mathrm{SVT}_{\lambda_{\mathrm{L}}}\left(\mathbf{L}_i^{k-1} - t^k \mathbf{R}_i^* \tau^* \mathbf{E}^*\left(\mathbf{E}\tau \sum_{j=1}^{n} (\mathbf{R}_j(\mathbf{L}_j^{k-1} + \mathbf{S}_j^{k-1})) - \mathbf{D}\right)\right) \\
\mathbf{S}_i^k &= \mathbf{T}^*\left[\Lambda_{\lambda_{\mathrm{S}}}\left(\mathbf{T}\left(\mathbf{S}_i^{k-1} - t^k \mathbf{R}_i^* \tau^* \mathbf{E}^*\left(\mathbf{E}\tau \sum_{j=1}^{n} (\mathbf{R}_j(\mathbf{L}_j^{k-1} + \mathbf{S}_j^{k-1})) - \mathbf{D}\right)\right)\right)\right].
\end{aligned} \tag{6}$$

For the simplicity in computation and representation, an ancillary variable $\mathbf{M}_i$ is introduced:

$$\mathbf{M}_i^{k-1} = \mathbf{L}_i^{k-1} + \mathbf{S}_i^{k-1} - t^k \mathbf{R}_i^* \tau^* \mathbf{E}^*\left(\mathbf{E}\tau \sum_{j=1}^{n} (\mathbf{R}_j(\mathbf{L}_j^{k-1} + \mathbf{S}_j^{k-1})) - \mathbf{D}\right). \tag{7}$$

Hence the iteration functions in Eq. (6) can be rewrote as

$$\begin{aligned}
\mathbf{L}_i^k &= \mathrm{SVT}_{\lambda_L}(\mathbf{M}_i^{k-1} - \mathbf{S}_i^{k-1}) \\
\mathbf{S}_i^k &= \mathbf{T}^*[\Lambda_{\lambda_S}(\mathbf{T}(\mathbf{M}_i^{k-1} - \mathbf{L}_i^{k-1}))].
\end{aligned} \tag{8}$$

Finally, the sliding motion compensated 4D image is assembled as $\sum_{j=1}^{n} (\mathbf{R}_j(\mathbf{L}_j + \mathbf{S}_j))$, and the free breathing 4D image reconstruction is obtained as $\tau \sum_{j=1}^{n} (\mathbf{R}_j(\mathbf{L}_j + \mathbf{S}_j))$.

3. Methods

The feasibility of SMC-LS has been validated using four different datasets: retrospectively undersampled liver 4D MRI phantom data with simulated free breathing, breath-hold and free-breathing liver 4D DCE-MRI phantom data, and in vivo free-breathing liver 4D MRI dataset. This study was institutional review board (IRB) approved and HIPAA compliant. Totally 11 healthy volunteers (6 males and 5 females, 20–30 years old) were imaged after obtaining informed consent. All the in vivo data were acquired using a 1.5 T scanner, 8-channel cardiac coil, multiphase spiral LAVA sequence with a 3D fast spoiled gradient echo stack of 48 golden angle variable density 2D spiral leaves per fully sampled volume [12,15]. For a fully sampled $k_x - k_y$ axial plane using 48 spiral leaves, the k-space was oversampled two-fold in the center (origin), whereas undersampled by a factor of 0.7 at the edge. 2D spiral leaves of the same angle were acquired consecutively and Cartesian encoded in k_z direction.

3.1. Simulation of respiratory sliding motion

To simulate abdominal organ motion in free-breathing digital phantom, we used a mathematical model proposed by Lujan et al [41,42] to generate periodic one dimensional sliding motion as follows:

$$x(t) = x_0 + A \cdot \cos^{2n}\left(\frac{\pi t}{T} - \phi_0\right) \tag{9}$$

where $x(t)$ is the position of an abdominal organ – such as the liver – at time t, A is the extent (amplitude) of the motion, T is the period of breathing cycle, n is a parameter determining the general shape of the model, and x_0, ϕ_0 are the starting position and the starting phase respectively. In our experiments, n was set to 2, T was set to 3.6 s. Since only the displacement of organ position was needed in our work, both x_0 and ϕ_0 were set to 0.

3.2. Liver 4D MRI phantom data with simulated free breathing

A fully sampled volume was acquired from a healthy volunteer with voxel size $1.33 \times 1.33 \times 4\,\mathrm{mm}^3$, and matrix size $256 \times 256 \times 50$. No contrast agent was used in this study, and the subject was instructed to hold breath at the end of natural inhalation before the starting of data acquisition. A static volumetric image was reconstructed using non-uniform IFFT of the fully sampled data. A sliding motion mask for the

static image was manually annotated using ITK-SNAP [38]. Then an animation of free-breathing volumes was created by applying the sliding motion generated by Eq. (9) to the abdominal organs inside the sliding interface. Totally 288 dynamic volumes, equivalent to 6 full sampling phases, were created for this digital phantom. Multi-coil spiral LAVA data were generated using the **E** operator in Eq. (3), which performs a multiplication by multi-channel coil sensitivities followed by an undersampled Fourier transform with golden angle spiral trajectories.

To evaluate the accuracy of sliding motion estimation, which is presented in Section 2.2, we created 5 digital phantoms with different amplitude of sliding motion, ranging from 4 to 20 mm, at a fixed step of 4 mm. To investigate the impact of motion estimation accuracy on image reconstruction quality, we compared the results of three different methods: the standard L + S reconstruction, SMC-LS with estimated sliding motion, SMC-LS with ground truth sliding motion. The PSNR was calculated as an objective metric for the evaluation of image reconstruction quality. Subjective assessment of reconstructed images was also performed by visually comparing with the ground truth images in different cross sections.

As a tradeoff between temporal resolution and quality resolution in both the standard L + S and SMC-LS reconstruction, one volume was reconstructed for every two 3D stacks of consecutive angled spiral leaves, leading to 144 reconstructed temporal frames. Correspondingly, the estimated sliding motion displacement signal was downsampled by a factor of 2. Other parameters were empirically determined and fixed in all experiments: $\lambda_{\mathbf{L}} = 0.01$, $\lambda_{\mathbf{S}} = 0.2$, iteration number = 100.

3.3. Breath-hold and free-breathing liver 4D DCE-MRI phantom data

In vivo DCE-MRI data were acquired from another healthy volunteer with voxel size $1.48 \times 1.48 \times 5\,mm^3$, and matrix size $256 \times 256 \times 36$. Gadopentetate dimeglumine (Gd-DTPA, Magnevist, Bayer HealthCare) was injected at a dose based on the subject's weight. The subject was instructed to hold breath at the end of natural inhalation as long as possible up to a total scan time of 50 s. Totally 4 full sampling phases, equivalent to 192 3D stacks of golden angle spiral leaves, were acquired.

A digital phantom for free-breathing liver 4D DCE-MRI was created as follows.

(1) 192 volumetric images were reconstructed using the standard L + S method with each volume for every 3D stack of spiral leaves.
(2) A composite volumetric image was reconstructed using non-uniform IFFT of all the acquired k-space data.
(3) A sliding motion mask was manually annotated in the composite image using ITK-SNAP [38].
(4) An animation of free-breathing volumes was created by adding masked sliding motion generated by Eq. (9) to the reconstructed breath-hold images using the sliding motion mask.
(5) Multi-coil spiral LAVA data were generated from the free-breathing volumes using the **E** operator in Eq. (3), which performs a multiplication by multi-channel coil sensitivities followed by an undersampled Fourier transform with golden angle spiral trajectories.

To quantitatively compare the reconstruction performance of the standard L + S and LASSI on motion-free liver 4D DCE-MRI data, a breath-hold digital phantom dataset was generated in a similar way but just with step 1 and 5 (skipping other steps). In both L + S and LASSI reconstruction, one volume was reconstructed for every two 3D stacks of consecutive angled spiral leaves, leading to 96 reconstructed temporal frames. Other parameters were empirically determined to obtain best overall subjective reconstruction quality and fixed in the following experiments. For the standard L + S reconstruction, the parameter setting was: $\lambda_{\mathbf{L}} = 0.01$, $\lambda_{\mathbf{S}} = 0.2$, and iteration number = 100. For LASSI reconstruction, the parameter setting was: $\lambda_{\mathbf{L}} = 600$, $\lambda_S = 0.025$, $\lambda_B = 6$, and iteration number = 100.

For free-breathing liver 4D DCE-MRI phantom data, reconstruction experiments were carried out using SMC-LS, the standard L + S, LASSI and XD-GRASP. The parameter setting for SMC-LS was the same as the standard L + S. For XD-GRASP reconstruction, two settings were used: (1) 4 respiratory states by 4 DCE states, totally 16 states; and (2) 6 respiratory states by 6 DCE states, totally 36 states.

3.4. In vivo free-breathing liver 4D MRI data

In vivo free-breathing liver 4D MRI data were acquired from 10 healthy volunteers (5 males and 5 females), including the one scanned for the creation of liver 4D MRI phantom data. No contrast agent was used in this study, and the subjects were instructed to keep natural free breathing. Totally 6 full sampling phases, equivalent to 288 3D stacks of golden angle spiral leaves, were acquired from each volunteer. The field of view was tuned for each individual so that it covered the whole liver during free breathing. Other parameters were: matrix size $256 \times 256 \times 48$–53, slice thickness 4 mm, and in plane resolution 1.34 to 1.56 mm.

Reconstruction experiments were carried out on this in vivo free-breathing liver 4D MRI data using SMC-LS and the standard L + S. One volume was reconstructed for every two 3D stacks of consecutive angled spiral leaves, leading to 144 reconstructed temporal frames for each subject. Other parameters were empirically determined and fixed in all experiments: $\lambda_{\mathbf{L}} = 0.01$, $\lambda_{\mathbf{S}} = 0.2$, iteration number = 100.

4. Results

4.1. Free-breathing liver 4D MRI phantom data

For quantitative evaluation of the sliding motion estimation method in SMC-LS, the Liver 4D MRI phantom data without contrast enhancement but with different depth of simulated free breathing were used. Fig. 1(a) shows a comparison between the estimated global displacement of sliding motion and the ground truth generated by Eq. (9) when $A = 12$ mm. The two motion signals are strongly correlated as they have similar periodic waveforms. But the estimated maximal range (~10 mm) was smaller than the ground truth. As shown in Fig. 1(b), the maximal range estimate increases almost linearly with increasing A but with a smaller slope.

Fig. 2 compares the PSNR of images reconstructed by the standard L + S and SMC-LS on this liver 4D MRI phantom data with different depth of simulated free breathing. SMC-LS achieved ~3 dB PSNR gain than the standard L + S reconstruction in each case. The improvement of image reconstruction quality could be attributed to the integration of sliding motion compensation into SMC-LS. Additional PSNR gain was observed when ground truth sliding motion was directly used in SMC-LS.

Fig. 3 visually compares the images reconstructed by the standard L + S and SMC-LS with corresponding ground truth images of the phantom in an example axial section and an example coronal section with zoomed-in ROIs. Compared to the standard L + S reconstruction, motion blurring artefacts are greatly reduced and image details are well preserved in SMC-LS reconstruction.

4.2. Breath-hold and free-breathing liver 4D DCE-MRI phantom data

Fig. 4 compares image slices reconstructed by the standard L + S and LASSI in an example axial section using the spiral sampled breath-hold liver 4D DCE-MRI phantom dataset. As seen from the residue images, LASSI obtained substantially lower reconstruction error than the standard L + S, with reference to the ground truth phantom images. In this experiment, the PSNR of LASSI reconstruction was 34.5 dB whereas the PSNR of standard L + S reconstruction was 31.3 dB.

Fig. 5 shows a visual comparison of the images reconstructed by the standard L + S, LASSI and SMC-LS with corresponding ground truth

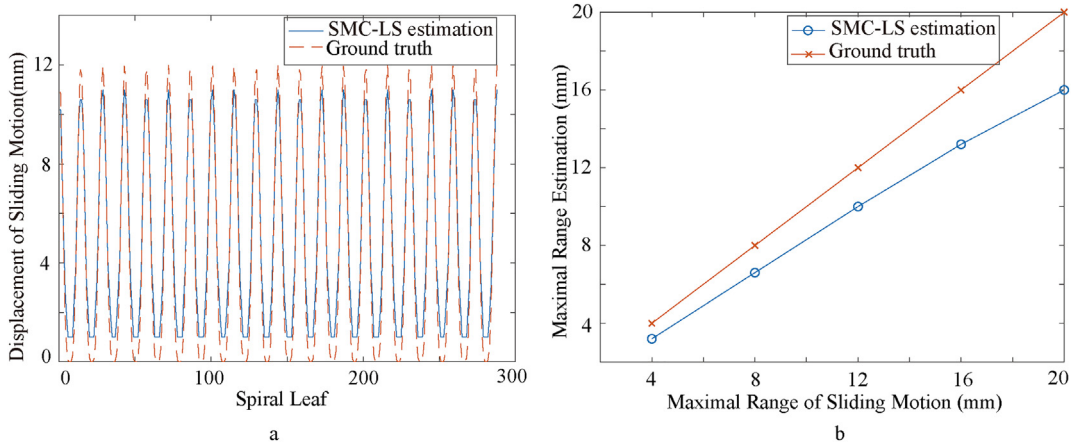

Fig. 1. Performance evaluation of the sliding motion estimation scheme used in SMC-LS on the spiral sampled free-breathing liver 4D MRI phantom dataset: (a) Estimated global displacement of sliding motion versus the ground truth when the maximal range was set to 12 mm, and (b) Estimated maximal range of sliding motion when the ground truth was set to 4–20 mm at a step of 4 mm. As shown in (a) and (b), the global displacement estimate has almost the same periodic waveform as the ground truth, but the maximal range is smaller than the ground truth, and the estimation error increases with increasing sliding motion range.

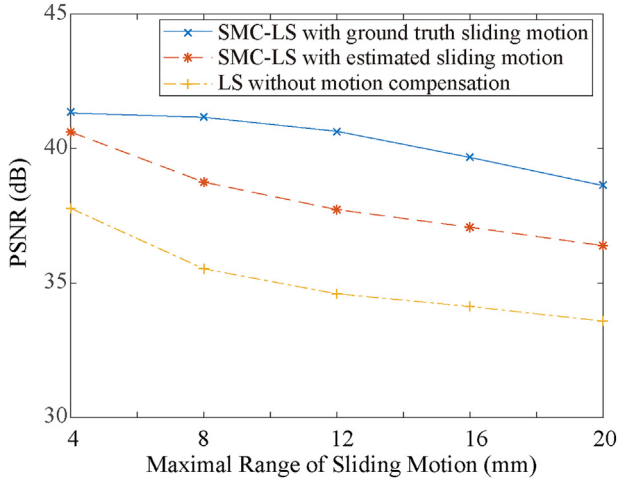

Fig. 2. Comparison of image reconstruction quality in terms of PSNR on the spiral sampled free-breathing liver 4D MRI phantom dataset with different maximal sliding motion ranges, from 4 to 20 mm at a step of 4 mm. The PSNR of the standard L + S without motion correction (indicated by the dash-dot line) decreased with increasing sliding motion range. The proposed SMC-LS reconstruction with estimated sliding motion (indicated by the dotted line) achieved ~3 dB PSNR gain in each case. Additional PSNR gain was observed when ground truth sliding motion was used in SMC-LS reconstruction (indicated by the solid line).

images of the free-breathing liver 4D DCE-MRI phantom in an example axial section and an example coronal section with zoomed-in ROIs. Compared to both the standard L + S and LASSI reconstruction, motion blurring artefacts are significantly reduced and spatial structures are well preserved in SMC-LS reconstruction. More importantly, contrast enhancement patterns are tracked more accurately in SMC-LS, as pointed out by the white arrows in the coronal view.

Fig. 6 visually compares the DCE images reconstructed by SMC-LS and XD-GRASP with different number of states. Using SMC-LS, 96 volumetric images were reconstructed, each of which corresponds to two consecutive 3D stacks of spirals, at a temporal resolution of ~0.6 s. When the k-space data were sorted into 4 DCE states by 4 motion states, XD-GRASP achieved similar image reconstruction quality as SMC-LS, but at the expense of much lower temporal resolution of ~3.6 s. When the temporal resolution was increased to 6 DCE states by 6 motion states, which was still lower than that of SMC-LS, the image reconstruction quality of XD-GRASP deteriorated seriously. As shown by the x-t profiles, SMC-LS reconstruction captured the temporal variations more clearly than XD-GRASP.

4.3. *In vivo free-breathing liver 4D MRI dataset*

SMC-LS and the standard L + S reconstruction were performed on in vivo free-breathing liver 4D MRI data acquired from 10 healthy volunteers. 144 temporal frames were reconstructed for each subject by each method. Fig. 7(a) compares reconstructed images of an example axial section and x-t profiles of a single line in case 1, and Fig. 7(b) shows the global displacement of sliding motion estimated by SMC-LS. Fig. 8 presents subjective comparisons in other six cases. Compared to the standard L + S reconstruction, motion blurring artefacts are effectively reduced and spatial structures are well preserved in SMC-LS reconstruction. The x-t profiles of the standard L + S and SMC-LS reconstruction both exhibit similar periodic variations as the estimated sliding motion, but SMC-LS reconstruction captured temporal variations more clearly, as pointed out by the white arrows.

5. Discussion

5.1. *Respiratory motion model*

Respiratory motion poses a lot of challenges on abdominal dynamic MRI reconstruction. An optical flow-based nonrigid motion model has been attempted in [34] to extend the standard L + S reconstruction for free-breathing dynamic MRI, where the motion field and image reconstruction are optimized alternately in iterations. However, the convergence of this alternating optimization is not guaranteed. In this paper, respiratory motion is simplified to its dominant component – global sliding of the internal abdominal organs. An important advantage is that the global displacement of sliding motion can be inferred directly from the acquired raw data. Therefore, image reconstruction iterations are decoupled from the complication of nonrigid motion estimation. As validated in this work, with global sliding motion compensation, motion blurring artefacts are significantly reduced in SMC-LS reconstruction. This improvement could be attributed to the recovery of inter-frame spatiotemporal correlations after sliding motion compensation.

Nevertheless, it is not trivial to infer an accurate respiratory motion signal directly from multi-coil raw data. As shown in Fig. 2, there is still space to improve image reconstruction quality in SMC-LS if we could further improve the accuracy of sliding motion estimation. On the other hand, as shown by the solid line in Fig. 2, even the ground truth

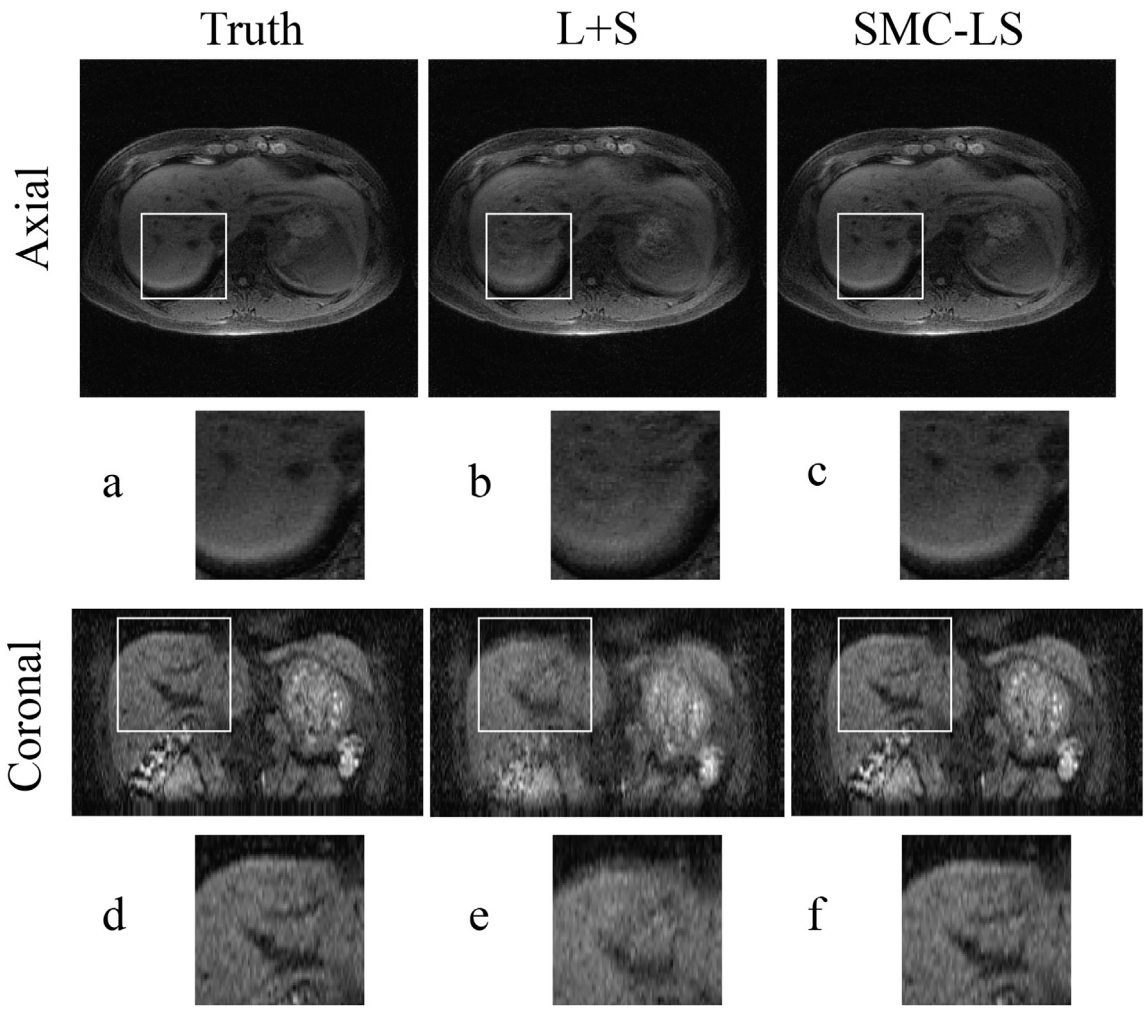

Fig. 3. Comparison of a ground truth image (left), its standard L + S reconstruction (middle) and SMC-LS reconstruction (right) in an example axial section (top) and an example coronal section (bottom) with zoomed-in ROIs on the spiral sampled free-breathing liver 4D MRI phantom dataset. One volumetric image was reconstructed for every two consecutive 3D stacks of spirals at a temporal resolution of ~0.6 s. Comparing SMC-LS with the standard L + S reconstruction, motion blurring artefacts were significantly reduced, and spatial structures were well preserved.

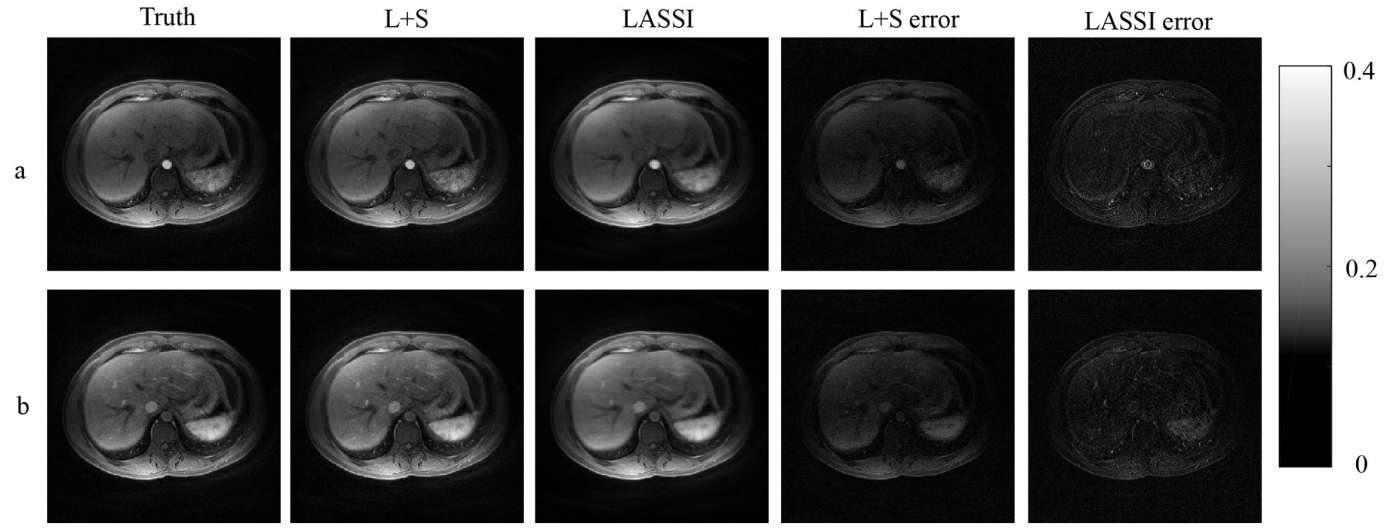

Fig. 4. Comparison of images reconstructed by standard L + S and LASSI in an example axial section using the spiral sampled breath-hold liver 4D DCE-MRI phantom dataset: (a) the top row and (b) the bottom row correspond to two different time points. One volumetric image was reconstructed for every two consecutive 3D stacks of spirals at a temporal resolution of ~0.6 s. It can be seen that LASSI reconstruction is a bit smoother with reduced noise/error compared to standard L + S reconstruction. In this experiment, the PSNR of LASSI reconstruction (34.5 dB) outperformed that of standard L + S reconstruction (31.3 dB).

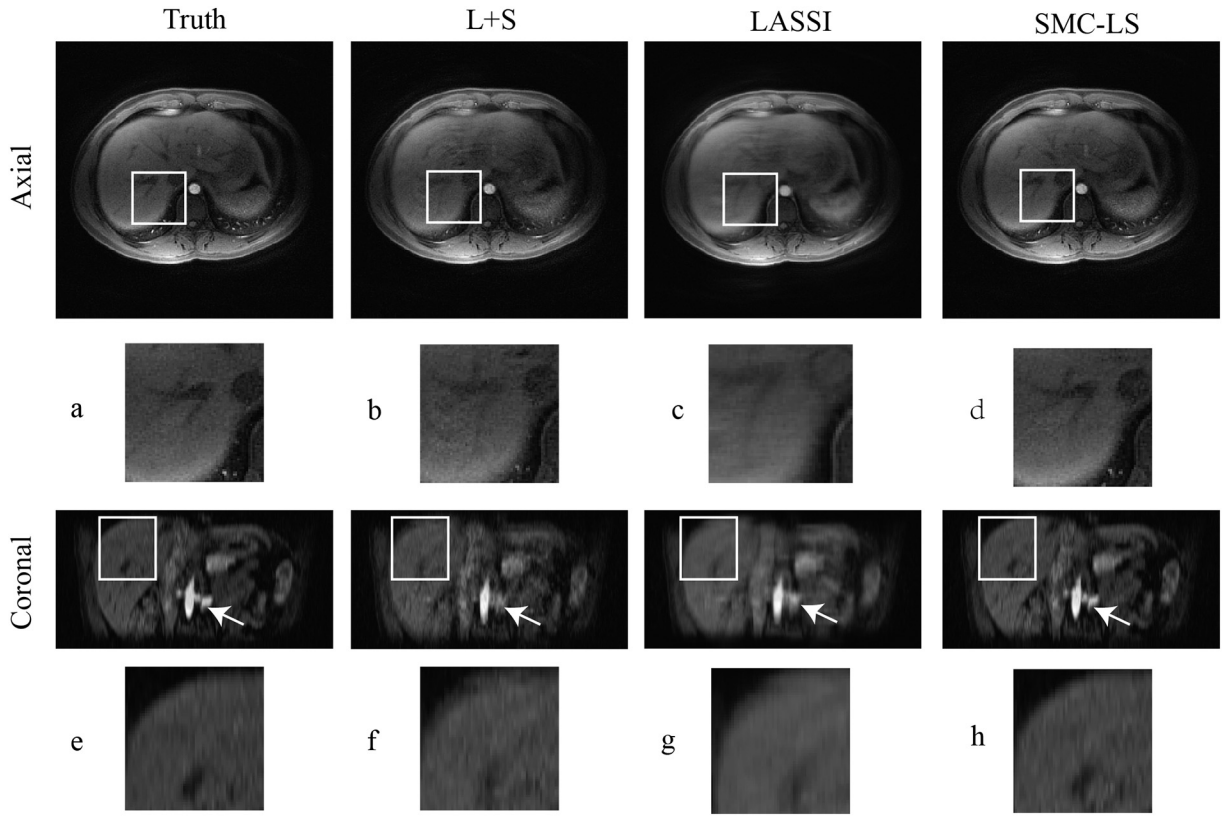

Fig. 5. Comparison of a ground truth image (1st column), its standard L + S reconstruction (2nd column), LASSI reconstruction (3rd column) and SMC-LS reconstruction (4th column) in an example axial section (top) and an example coronal section (bottom) with zoomed-in ROIs on the spiral sampled free-breathing liver 4D DCE-MRI phantom dataset. One volumetric image was reconstructed for every two consecutive 3D stacks of spirals at a temporal resolution of ~0.6 s. Comparing SMC-LS with both the standard L + S reconstruction and LASSI reconstruction, motion blurring artefacts were significantly reduced, spatial structures were well preserved, and contrast enhancement patterns were tracked more accurately (see white arrows in the coronal view).

displacement is used in sliding motion compensation, image reconstruction quality decreases with increasing motion range. This is probably due to the imperfect segmentation of the sliding motion mask and the error introduced by motion transformation τ in case of large displacement. Fortunately, when the maximal rang of sliding motion is moderate, which is common in natural free breathing, quality loss is small.

In fact, the respiratory motion of abdominal inner organs is more complicated than the oversimplified global sliding motion model, as presented in liver MR registration [43]. Besides the constraints on the maximal range of sliding motion, there are two other limitations for successful application of the proposed SMC-LS reconstruction to clinical liver DCE-MRI exams. First, the subject has to keep quiet breathing in order to minimize the in-outward motion of the abdominal wall during data acquisition so that a static sliding motion mask could be used throughout the image sequence reconstruction. Second, the imaging coordinate system should be setup properly such that the breathing induced sliding motion is majorly along one dimension. Otherwise the image quality of SMC-LS reconstruction would be compromised when these constraints are not satisfied in real exams.

In addition, the proposed global sliding motion compensation technique could be potentially extended to other applications, e.g. abdominal image registration. The respiratory sliding motion of abdominal internal organs violates the conventional homogeneous smoothness regularization and commonly makes the registration accuracy compromised [43]. By applying prior sliding motion compensation, the motion discontinuity between the image pair would be greatly reduced so that conventional nonrigid registration with homogeneous smoothness regularization could be used for abdominal image registration. We will investigate this further in our future study.

5.2. Comparison with state-of-the-art

In natural free breathing, respiratory motion is nearly periodic. As compared in Figs. 7 and 8, both the standard L + S reconstruction and SMC-LS reconstruction could capture similar periodic temporal variations in free-breathing liver 4D dynamic MRI without contrast enhancement. In fact, the standard L + S reconstruction works well when the motion magnitude is small enough, e.g. in cardiac imaging. However, for larger motion as in free breathing, the images reconstructed by the standard L + S method are blurry and the motion captured is smaller than the ground truth. After global sliding motion compensation for the internal abdominal organs, the residue motion is small enough to use the standard L + S reconstruction to obtain satisfactory results.

For DCE-MRI, highly temporal resolved contrast enhancement tracking is essential for clinical diagnosis. In XD-GRASP, image reconstruction quality deteriorates when the acquired k-space data are distributed into more states, because less data in each state leads to more undersampling artefacts. When less states are used in XD-GRASP, motion dynamics and contrast enhancement pattern are smoothed by lower temporal resolution. Therefore, a delicate determination of state number is required in XD-GRASP reconstruction to optimize image quality. As shown in Fig. 6, SMC-LS outperforms XD-GRASP with sub-second temporal resolution while maintaining a good image quality.

As evaluated in Section 4.2, LASSI reconstruction [20] outperformed the standard L + S reconstruction [19] in breath-hold liver 4D DCE-MRI (Fig. 4). This could be attributed to the introduction of an adaptive sparse signal model based on dictionary learning. However, the image quality of LASSI reconstruction is still compromised for free-breathing data (Fig. 5) due to lack of explicit respiratory motion

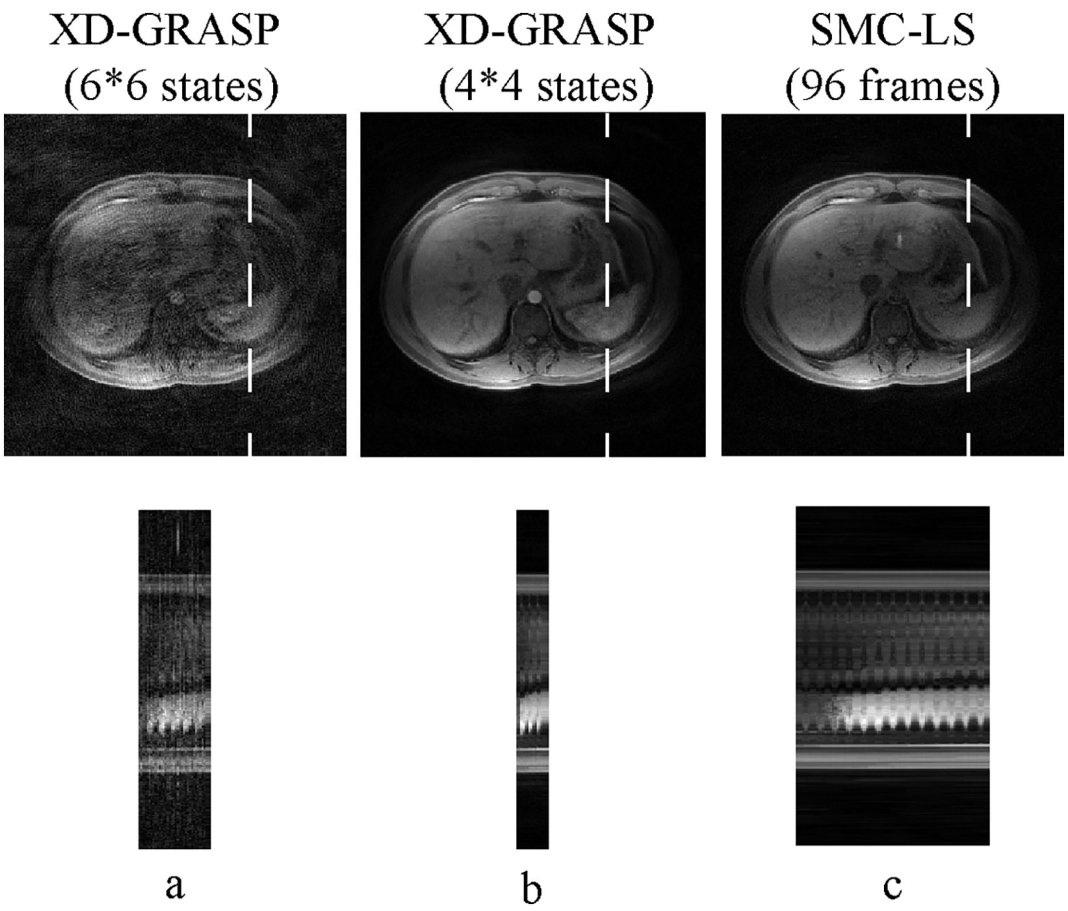

Fig. 6. Comparison of the temporal profiles (bottom) in a single cross-section indicated by the dashed lines in an example axial section (top) reconstructed by (a) XD-GRASP with 6 DCE states by 6 motion states, (b) XD-GRASP with 4 DCE states by 4 motion states, and (c) SMC-LS with 96 frames for the spiral sampled free-breathing liver 4D DCE-MRI phantom dataset. XD-GRASP reconstruction using 16 states obtained significantly improved image quality than using 36 states but at the expense of lower temporal resolution. SMC-LS reconstruction with 96 frames achieved higher temporal resolution than XD-GRASP reconstruction with 36 states while maintaining similar image quality as XD-GRASP reconstruction with 16 states. The x-t profiles show that SMC-LS reconstruction captured the temporal variations more clearly than XD-GRASP reconstruction.

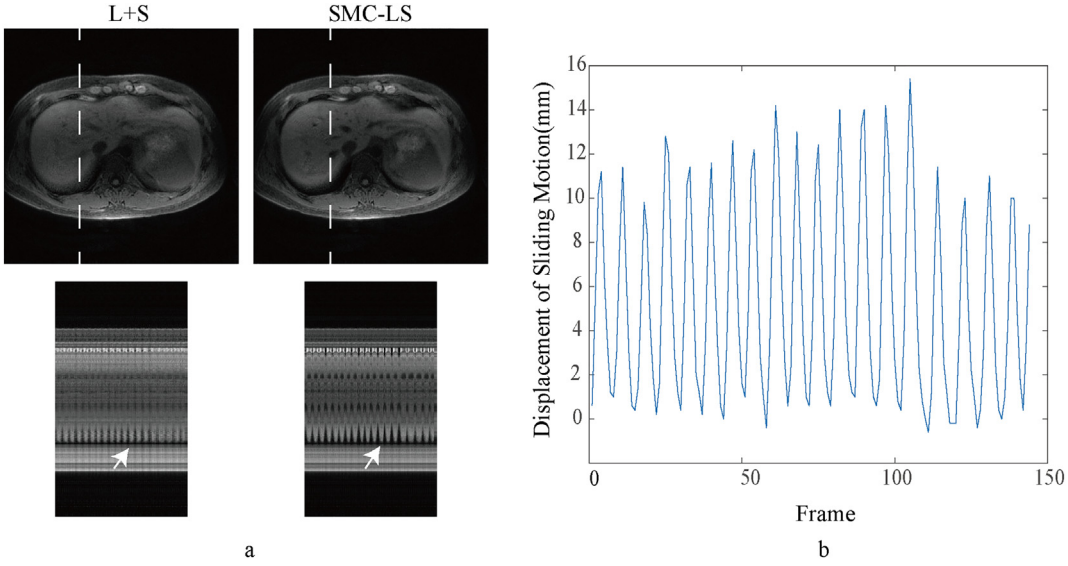

Fig. 7. Results for case 1 of the spiral sampled in vivo free-breathing liver 4D MRI dataset: (a) comparison of the temporal profiles (bottom) in a single cross-section indicated by the dashed lines in an example axial section (top) reconstructed by the standard L + S and SMC-LS respectively, both with 144 frames at a temporal resolution of ~0.6 s, and (b) global displacement of sliding motion estimated by SMC-LS. The temporal profiles of the standard L + S and SMC-LS reconstruction both exhibit similar periodic variations as the estimated sliding motion, but SMC-LS reconstruction captured temporal variations more clearly.

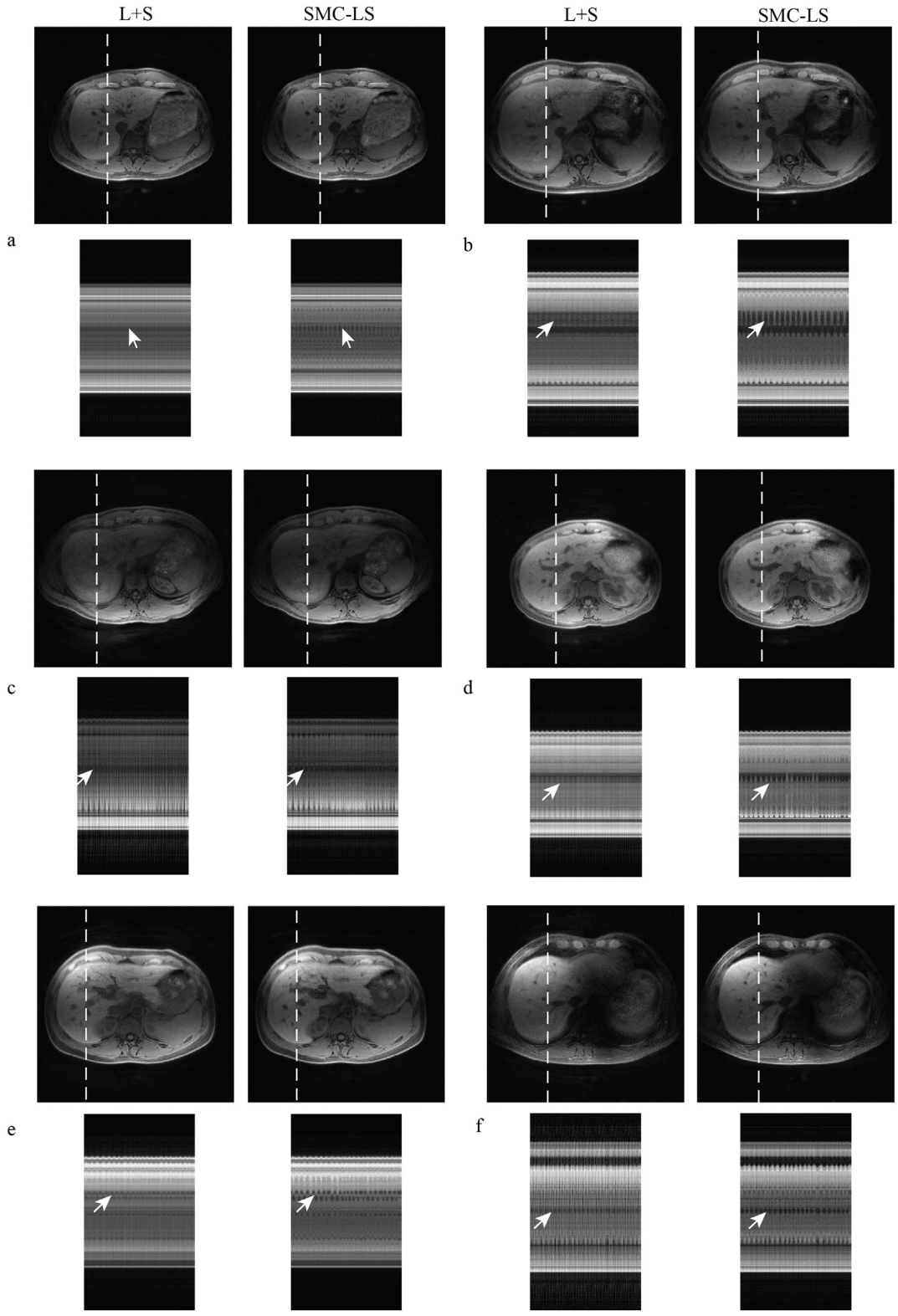

Fig. 8. Comparison of image reconstruction in other six cases of the spiral sampled in vivo free- breathing liver 4D MRI dataset. (a)–(f) correspond to case 2–7 respectively. Each subfigure shows a comparison of the temporal profiles (bottom) in a single cross-section indicated by the dashed lines in an example axial section (top) reconstructed by the standard L + S (left) and SMC-LS (right) respectively, both with 144 frames at a temporal resolution of ~0.6 s. The temporal profiles of the standard L + S and SMC-LS reconstruction both exhibit similar periodic variations, but SMC-LS reconstruction captured temporal variations more clearly.

correction. We will investigate the potential to improve image reconstruction quality of SMC-LS for free-breathing liver 4D DCE-MRI by transferring the proposed sliding motion compensation mechanism from the standard L + S to more advanced L + S framework, e.g. LASSI, in our future work.

5.3. Choice of regularization parameters

The setting of regularization parameters λ_L and λ_S is crucial to the optimization results of the standard L + S reconstruction and SMC-LS reconstruction problems formulated in Eqs. (2) and (3). In this work, we used an empirical method to determine the optimal parameter setting by subjectively assessing image reconstruction quality when parameters λ_L and λ_S were varied over a range of possible values. We observed that for both the standard L + S reconstruction and the proposed SMC-LS reconstruction, larger λ_L, λ_S would smooth the **L**, **S** component, whereas smaller λ_L, λ_S would bring more noise into the **L**, **S** component, respectively. And the ratio of λ_L/λ_S would balance the separation between **L** and **S**. According to the analogy between Eqs. (2) and (3), it is understandable that image reconstruction quality undergoes similar changes for both methods under the same setting of λ_L and λ_S. For results presented in this work, we have chosen a fixed setting of $\lambda_L = 0.01$ and $\lambda_S = 0.2$, which yielded the best overall subjective image reconstruction quality for both methods.

6. Conclusion

A novel method called SMC-LS is introduced for high spatio-temporal free-breathing whole-liver 4D DCE-MRI reconstruction. Global sliding of the internal abdominal organs is modeled as the major component of respiratory motion and inferred directly from the undersampled raw data. By incorporating sliding motion compensation into the standard L + S reconstruction, the reconstructed temporal frames are roughly registered for L + S decomposition. Results on phantom data and in vivo data demonstrated that SMC-LS reconstruction can preserve high resolution spatial structures and capture clear temporal variations at a sub-second frame rate for free-breathing liver 4D DCE-MRI.

Supplementary data to this article can be found online at https://doi.org/10.1016/j.mri.2019.01.012.

Acknowledgements

This research was supported in part by the U.S. National Institutes of Health under Grant R01 CA181566, R01 EB013443, and R01 NS090464.

References

[1] Ronot M, Lambert S, Daire JL, Lagadec M, Doblas S, Garteiser P, et al. Can we justify not doing liver perfusion imaging in 2013? Diagn Interv Imaging 2013;94(12):1323–36.
[2] Sodickson DK, Manning WJ. Simultaneous acquisition of spatial harmonics (SMASH): fast imaging with radiofrequency coil arrays. Magn Reson Med 1997;38(4):591–603.
[3] Pruessmann KP, Weiger M, Scheidegger MB, Boesiger P, et al. SENSE: sensitivity encoding for fast MRI. Magn Reson Med 1999;42(5):952–62.
[4] Griswold MA, Jakob PM, Heidemann RM, Nittka M, Jellus V, Wang J, et al. Generalized autocalibrating partially parallel acquisitions (GRAPPA). Magn Reson Med 2002;47(6):1202–10.
[5] Tsao J, Boesiger P, Pruessmann KP. k-t BLAST and k-t SENSE: dynamic MRI with high frame rate exploiting spatiotemporal correlations. Magn Reson Med 2003;50(5):1031–42.
[6] Xu D, King KF, Liang Z. Improving k-t SENSE by adaptive regularization. Magn Reson Med 2007;57(5):918–30.
[7] Huang F, Akao J, Vijayakumar S, Duensing GR, Limkeman M. k-t GRAPPA: a k-space implementation for dynamic MRI with high reduction factor. Magn Reson Med 2005;54(5):1172–84.
[8] Xie J, Lai P, Huang F, Li Y, Li D. Cardiac magnetic resonance imaging using radial k-space sampling and self-calibrated partial parallel reconstruction. Magn Reson Imaging 2010;28(4):495–506.
[9] Delattre BMA, Heidemann RM, Crowe LA, Vallée J-P, Hyacinthe J-N. Spiral demystified. Magn Reson Imaging 2010;208(6):862–81.
[10] Jung H, Sung K, Nayak KS, Kim EY, Ye JC. k-t FOCUSS: A general compressed sensing framework for high resolution dynamic MRI. Magn Reson Med 2009;61(1):103–16.
[11] Miao J, Guo W, Narayan S, Wilson DL. A simple application of compressed sensing to further accelerate partially parallel imaging. Magn Reson Imaging 2013;31(1):75–85.
[12] Xu B, Spincemaille P, Chen G, Agrawal M, Nguyen TD, Prince MR, et al. Fast 3D contrast enhanced MRI of the liver using temporal resolution acceleration with constrained evolution reconstruction. Magn Reson Med 2013;69(2):370–81.
[13] Feng L, Grimm R, Block KT, Chandarana H, Kim S, Xu J, et al. Golden-angle radial sparse parallel MRI: combination of compressed sensing, parallel imaging, and golden-angle radial sampling for fast and flexible dynamic volumetric MRI. Magn Reson Med 2014;72(3):707–17.
[14] Li Q, Qu X, Liu Y, Guo D, Lai Z, Ye J, et al. Accelerating patch-based directional wavelets with multicore parallel computing in compressed sensing MRI. Magn Reson Imaging 2015;33(5):649–58.
[15] Cooper MA, Nguyen TD, Xu B, Prince MR, Elad M, Wang Y, et al. Patch based reconstruction of undersampled data (PROUD) for high signal-to-noise ratio and high frame rate contrast enhanced liver imaging. Magn Reson Med 2015;74(6):1587–97.
[16] Iyer SK, Tasdizen T, Burgon N, Kholmovski E, Marrouche N, Adluru G, et al. Compressed sensing for rapid late gadolinium enhanced imaging of the left atrium: a preliminary study. Magn Reson Imaging 2016;34(7):846–54.
[17] Majumdar A, Ward RK, Aboulnasr T. Non-convex algorithm for sparse and low-rank recovery: application to dynamic MRI reconstruction. Magn Reson Imaging 2013;31(3):448–55.
[18] Majumdar A. Improved dynamic MRI reconstruction by exploiting sparsity and rank-deficiency. Magn Reson Imaging 2013;31(5):789–95.
[19] Otazo R, Candès E, Sodickson DK. Low-rank plus sparse matrix decomposition for accelerated dynamic MRI with separation of background and dynamic components. Magn Reson Med 2015;73(3):1125–36.
[20] Ravishankar S, Moore BE, Nadakuditi RR, Fessler JA. Low-rank and adaptive sparse signal (LASSI) models for highly accelerated dynamic imaging. IEEE Trans Med Imaging 2017;36(5):1116–28.
[21] Schultz CL, Alfidi RJ, Nelson AD, Kopiwoda SY, Clampitt ME. The effect of motion on two-dimensional Fourier transformation magnetic resonance images. Radiology 1984;152(1):117–21.
[22] Axel L, Summers RM, Kressel HY, Charles C. Respiratory effects in two-dimensional Fourier transform MR imaging. Radiology 1986;160(3):795–801.
[23] Paling MR, Brookeman JR. Respiration artifacts in MR imaging: reduction by breath holding. J Comput Assist Tomogr 1986;10(6):1080–2.
[24] Feinberg DA, Rofsky NM, Johnson G. Multiple breath-hold averaging (mba) method for increased snr in abdominal MRI. Magn Reson Med 1995;34(6):905–9.
[25] Liu J, Spincemaille P, Codella NC, Nguyen TD, Prince MR, Wang Y. Respiratory and cardiac self-gated free-breathing cardiac CINE imaging with multiecho 3D hybrid radial SSFP acquisition. Magn Reson Med 2010;63(5):1230–7.
[26] Du H, Lam F. Compressed sensing MR image reconstruction using a motion-compensated reference. Magn Reson Imaging 2012;30(7):954–63.
[27] Ahmed AH, Qureshi IM, Shah JA, Zaheer M. Motion correction based reconstruction method for compressively sampled cardiac MR imaging. Magn Reson Imaging 2017;36:159–66.
[28] Tolouee A, Alirezaie J, Babyn P. Nonrigid motion compensation in compressed sensing reconstruction of cardiac cine MRI. Magn Reson Imaging 2018;46:114–20.
[29] Lingala SG, DiBella E, Jacob M. Deformation corrected compressed sensing (DC-CS): a novel framework for accelerated dynamic MRI. IEEE Trans Med Imaging 2015;34(1):72–85.
[30] Yoon H, Kim KS, Kim D, Bresler Y, Ye JC. Motion adaptive patch-based low-rank approach for compressed sensing cardiac cine MRI. IEEE Trans Med Imaging 2014;33(11):2069–85.
[31] Tolouee A, Alirezaie J, Babyn P. Motion-compensated data decomposition algorithm to accelerate dynamic cardiac MRI. Magn Reson Mater Phys 2018;31(1):33–47.
[32] Shechter G, Ozturk C, Resar JR, McVeigh ER. Respiratory motion of the heart from free breathing coronary angiograms. IEEE Trans Med Imaging 2004;23(8):1046–56.
[33] Fink C. Analysis of intrathoracic tumor mobility during whole breathing cycle by dynamic MRI. Int J Radiat Oncol 2004;59(4):952–9.
[34] Otazo R, Koesters T, Candes EJ, Sodickson DK. Motion-guided low-rank plus sparse (L+ S) reconstruction for free-breathing dynamic MRI. Proc Int Soc Magn Reson Med 2014:0742.
[35] Zhang T, Cheng JY, Potnick AG, Barth RA, Alley MT, Uecker M, et al. Fast pediatric 3D free-breathing abdominal dynamic contrast enhanced MRI with high spatio-temporal resolution. J Magn Reson Imaging 2015;41(2):460–73.
[36] Feng L, Axel L, Chandarana H, Block KT, Sodickson DK, Otazo R. XD-GRASP: Golden-angle radial MRI with reconstruction of extra motion-state dimensions using compressed sensing. Magn Reson Med 2016;75(2):775–88.
[37] Candès EJ, Li X, Ma Y, Wright J. Robust principal component analysis? J ACM 2011;58(3):1–37.
[38] Yushkevich PA, Piven J, Hazlett HC, Smith RG, Ho S, Gee JC, et al. User-guided 3D active contour segmentation of anatomical structures: significantly improved efficiency and reliability. NeuroImage 2006;31(3):1116–28.
[39] Wang H, Dong L, O'Daniel J, Mohan R, Garden AS, Ang KK, et al. Validation of an accelerated 'demons' algorithm for deformable image registration in radiation therapy. Phys Med Biol 2005;50(12):2887.
[40] Zhang T, Cheng JY, Chen Y, Nishimura DG, Pauly JM, Vasanawala SS. Robust self-

navigated body MRI using dense coil arrays. Magn Reson Med 2016;76(1):197–205.
[41] Lujan AE, Larsen EW, Balter JM, Ten Haken RK. A method for incorporating organ motion due to breathing into 3D dose calculations. Med Phys 1999;26(5):715–20.
[42] Lujan AE, Balter JM, Ten Haken RK. A method for incorporating organ motion due to breathing into 3D dose calculations in the liver: sensitivity to variations in motion. Med Phys 2003;30(10):2643–9.
[43] Li D, Zhong W, Deh KM, Nguyen TD, Prince MR, Wang Y, Spincemaille P. Discontinuity preserving liver MR registration with 3D active contour motion segmentation. IEEE Trans Biomed Eng, early access 2018 10.1109/TBME.2018.2880733.